Global bifurcations and bistability at the locking boundaries of a semiconductor laser with phase-conjugate feedback

Kirk Green and Bernd Krauskopf
Department of Engineering Mathematics, University of Bristol, Bristol BS8 1TR, United Kingdom
(Received 26 September 2001; revised manuscript received 4 February 2002; published 30 July 2002)

We investigate dynamics and bifurcations of a single-mode semiconductor laser subject to phase-conjugate feedback near the locking region. The system is described by rate equations which are a three-dimensional system with a delay. With tools that go much beyond mere simulation, we find and follow steady states regardless of their stability and compute unstable manifolds of saddle points. Furthermore, we identify heteroclinic bifurcations, which turn out to be responsible for bistability and excitability at the locking boundaries.

DOI: 10.1103/PhysRevE.66.016220 PACS number(s): 05.45.Xt, 05.45.Gg, 42.65.−k

I. INTRODUCTION

Recently there has been much interest in the nonlinear dynamics of semiconductor lasers; see, for example, the recent overviews, Refs. [1,2], and further references therein. Due to the material properties of semiconductor lasers, external influences can alter the stability and dynamics of the laser dramatically. Knowledge of this effect is therefore essential for physical applications. Of particular interest are lasers subject to optical feedback, such as lasers with conventional optical feedback (COF) from an external mirror [3,4], lasers with phase conjugate feedback [5–10], the case considered here, lasers with optoelectronic feedback [11], and mutually coupled lasers with delay [12]. In all these cases the relevant and generally well-established models are delay differential equations (DDEs) [13].

Delay differential equations have received a lot of attention recently. Other areas where DDEs are crucial include biology [14], neural networks [15], and control theory [16]. It is quite a challenge to understand the dynamics and bifurcations of a DDE. Already in the case of one fixed delay τ (like in a laser with feedback), the phase space of the DDE is the infinite-dimensional space of continuous functions on the delay interval $[-\tau,0]$; see Ref. [17]. Tackling delay equations arising in applications is analytically very hard, and for a long time the only numerical tool was direct simulation by integration of the DDE. Very recently the package DDE-BIFTOOL [18] was developed, allowing numerical continuation of steady states and periodic solutions and the detection of their local bifurcations. Building on this work, we developed a method for computing unstable manifolds in DDEs. These tools allow one to find global bifurcations that are responsible for sudden changes of the observed dynamics of a DDE.

In this paper we bring these tools to bear to study the locking mechanism in a semiconductor laser receiving *phase-conjugate feedback* (PCF) from a phase-conjugating mirror (PCM) [7,9,10]. Experimentally, PCF can be generated by degenerate four-wave mixing, a nonlinear process that can be achieved by counter propagating laser beams in atomic vapors or a semiconductor material, or by using gratings or optic crystals [5,19,20]. Phase-conjugate feedback is physically interesting as it produces a return wave that coincides exactly with the incident wave, so that alignment is less of an issue. Furthermore, distortions are undone on the return trip in the external cavity. A laser with PCF was shown to exhibit complicated nonlinear dynamics, including stable periodic operation, quasiperiodic motion and chaos, as was found in detailed simulations of bifurcation diagrams, phase plots, and optical spectra. The overall picture is that of regions of periodic output that are interspersed with ''bubbles'' of chaos [9,10].

Here we concentrate on the mechanism of locking. Physically, in its locking range the PCF laser is both frequency locked and phase locked to the frequency of the PCM pump laser. Unlike the case of a COF laser, phase locking in a PCF laser does not depend on the feedback phase. In particular, phase locking results in an ultranarrow laser linewidth that has been shown to be stable even with the addition of noise [9]. By continuing steady states and computing the unstable manifolds of saddle points we find that hysteresis loops and global bifurcations are involved in the mechanism of locking in the PCF laser.

II. RATE EQUATIONS

Our object of study is a single-mode PCF laser receiving feedback from a PCM that responds instantaneously, as is shown schematically in Fig. 1. The length of the laser is typically less than 1 mm, while the length of the external cavity L can be several centimeters to 1 m, leading to typical delay times $\tau=2L/c$ in the range of 0.4 ns to 7.0 ns.

The rate equations describing this PCF laser are well established [7,9,10] and can be written as

$$\begin{aligned}\frac{dE}{dt} &= \frac{1}{2}\left[-i\alpha G_N[N(t)-N_{\mathrm{sol}}]+\left(G(t)-\frac{1}{\tau_p}\right)\right]E(t)\\ &\quad+\kappa E^*(t-\tau)\exp[i\phi_{\mathrm{PCM}}],\\ \frac{dN}{dt} &= \frac{I}{q}-\frac{N(t)}{\tau_e}-G(t)|E(t)|^2\end{aligned} \tag{1}$$

for the evolution of the slowly varying complex electric field $E(t)=E_x(t)+iE_y(t)$ and the population inversion $N(t)$. In system (1), nonlinear gain is included as $G=G_N(N(t)-N_0)(1-\epsilon P(t))$, where $\epsilon=3.57\times10^{-8}$ is the nonlinear gain coefficient and $P(t)=|E(t)|^2$ is the intensity. This produces an effective detuning of 166 MHz. Parameter values are set to realistic values [10], namely, the line-width

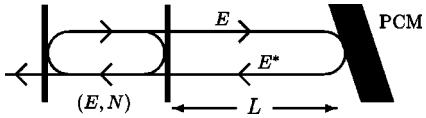

FIG. 1. Sketch of a semiconductor laser with phase-conjugate feedback.

enhancement factor $\alpha=3$, the optical gain $G_N=1190\ \mathrm{s}^{-1}$, the photon lifetime $\tau_p=1.4$ ps, the injection current $I=65.1$ mA, the magnitude of the electron charge $q=1.6\times10^{-19}$ C, the electron lifetime $\tau_e=2$ ns, and the transparency electron number $N_0=1.64\times10^8$. The phase shift ϕ_{PCM} at the PCM was set to zero and $N_{\mathrm{sol}}=N_0+1/(G_N\tau_p)$. The feedback term in system (1) involves the feedback rate κ and the external cavity round-trip time τ, which we fix at $\tau=2/3$ ns. Together they form the dimensionless bifurcation parameter $\kappa\tau$.

System (1) is written in the frame of reference of the solitary laser. A locked solution is the one where the frequency of the PCM pump laser is locked to that of the solitary laser and, therefore, locked solutions are steady states of system (1). Note that noise terms due to spontaneous emission have been left off system (1). It has been shown that both intensity and frequency noise are negligible at the low frequency range we are dealing with [7].

Mathematically, system (1) is a system of DDEs [17]. The state of the system at time $t>0$ is a continuous function on the time interval $[t-\tau,t]$, which is an evolution of the initial condition defined on the time interval $[-\tau,0]$. Therefore, the system is infinite dimensional. While (E,N)-space is not the phase space of system (1), it is nevertheless helpful to show the dynamics projected onto (E,N)-space, which is also called the physical space of system (1).

System (1) is symmetric under the transformation $E\rightarrow -E$, which corresponds to a rotation of π of the E-plane, so that an attractor is either symmetric, or has a symmetric counterpart [10,21]. Physically, this symmetry corresponds to a phase shift by π. The symmetry implies restrictions on the types of bifurcations of periodic solutions: for example, symmetric periodic solutions cannot undergo period-doubling bifurcations [22]. More generally, this discrete symmetry allows for the possibility of symmetry-breaking bifurcations. Note that the PCF laser considered here is different from the COF laser in terms of the underlying symmetry of the governing equations [21]. The COF laser is symmetric under any rotation of the electric field E and does not feature symmetry-breaking bifurcations.

III. COMPUTATIONAL METHODS FOR DDEs

In our study we make use of very recent developments in theory and numerical methods for DDEs. In simulations we integrate system (1) with an Adams-Bashforth fourth-order multistep method. Moreover, we use recently developed tools for DDEs that go beyond simulation.

First, we use the continuation package DDE-BIFTOOL [18], consisting of Matlab routines, for the bifurcation analysis of steady states and periodic solutions. This not only allows one to find and follow stable solutions (those one also finds by simulation), but also unstable ones. Furthermore, DDE-BIFTOOL detects local bifurcations, including saddle-node bifurcations, Hopf bifurcations, period-doubling bifurcations, and saddle-node bifurcations of limit cycles. The continuation of bifurcations leading to mixed-mode oscillations of a COF laser in Ref. [23] and our bifurcation analysis of the PCF laser here and in Ref. [24] are first examples of continuation studies with DDE-BIFTOOL.

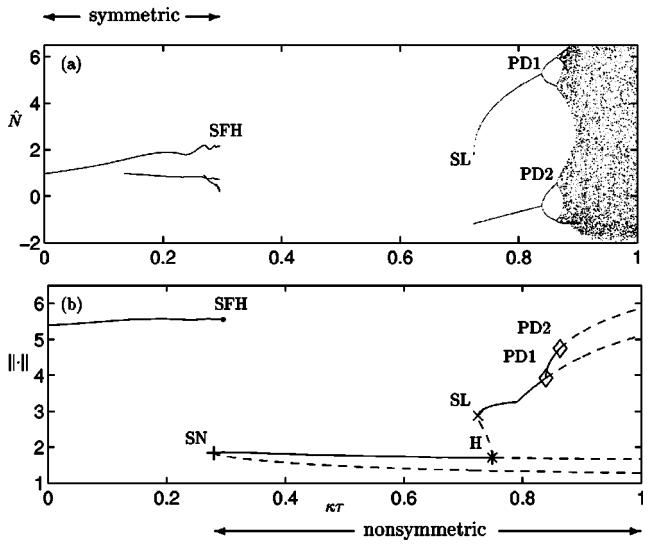

FIG. 2. Bifurcation diagram, obtained by simulation showing normalized inversion $\hat{N}$ versus the feedback strength $\kappa\tau$ (a), and computed with DDE-BIFTOOL showing a normalized amplitude versus $\kappa\tau$ (b); see text for details.

Second, we compute the one-dimensional (1D) unstable manifolds of saddle steady states with one unstable eigenvalue. Each 1D unstable manifold has two branches, which are computed by integrating from two initial conditions along the associated 1D unstable eigendirection close to but on different sides of the steady state. This eigendirection can be found by an iterative approach [25] or with a routine that was recently added to DDE-BIFTOOL. Knowing at which attractor the branches of 1D unstable manifolds end up is crucial for understanding the global dynamics, as will become clear in Sec. V.

IV. BIFURCATION DIAGRAMS

Figure 2 contains two bifurcation diagrams. In Fig. 2(a) we integrated system (1) and plotted (after transients died away) the normalized value of the inversion $\hat{N}=(N/N_{sol}-1)\times10^3$ whenever the intensity P crossed its average value in the positive direction [10]. The region with no points corresponds to a locked solution, a small number of points correspond to a periodic solution, and a large number of points correspond to chaotic dynamics. Due to the presence of hysteresis discussed below, the periodic solution for $\kappa\tau\in[0.0000,0.2953]$ was computed for increasing $\kappa\tau$, while the periodic solution for $\kappa\tau\in[0.7487,0.9004]$ was computed for decreasing $\kappa\tau$.

Figure 2(b) was obtained with DDE-BIFTOOL. For steady states we plot $\mathrm{Re}(E)$ and for periodic solutions we

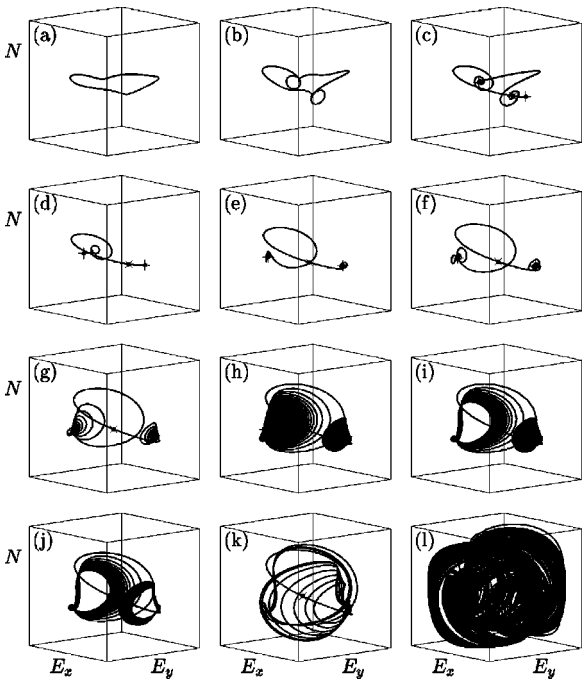

FIG. 3. Phase portraits shown in projection onto (E,N)-space. Except for (a) and (b), plotted are both branches of the 1D unstable manifold of one of the two symmetric saddle points ($\times$). The box is $[-200,200]\times[-200,200]\times[7.61\times10^8,7.68\times10^8]$; from (a) to (l), $\kappa\tau$ takes the values 0.1000, 0.2700, 0.2952, 0.3065, 0.4410, 0.5180, 0.6182, 0.7183, 0.7252, 0.7253, 0.7904, and 0.9004.

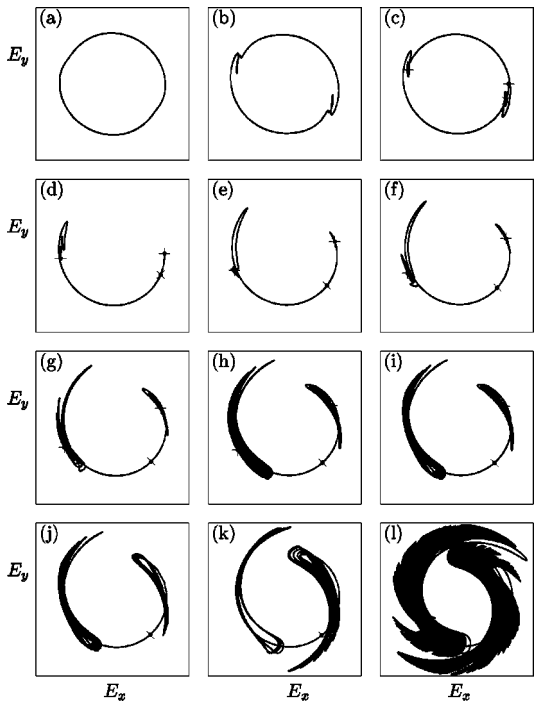

FIG. 4. Projection of plots in Fig. 3 onto the E-plane; the square is $[-270,270]\times[-270,270]$.

plot $|\max[\mathrm{Re}(E)]-\min[\mathrm{Re}(E)]|$, offset by the $\mathrm{Re}(E)$ value of the steady states at the Hopf point. Attracting solutions are drawn as solid curves, while unstable solutions are drawn as dashed curves. By studying the eigenvalues of the system we are able to identify the bifurcations involved, namely a saddle-node bifurcation (SN), a Hopf bifurcation (H), period-doubling bifurcations (PD), and a saddle-node bifurcation of limit cycles (SL). A global saddle-focus heteroclinic (SFH) bifurcation was observed at $\kappa\tau\approx0.2953$. The one-dimensional unstable manifold of one saddle approaches the other saddle along its stable manifold in a spiralling fashion. In light of the symmetry of system (1), this is the case of a Shil'nikov bifurcation with negative saddle quantity, that is, not involving horseshoe dynamics; see Ref. [22] and Sec. VI A. The symmetry of solution branches, which can be found from the respective phase portraits, is indicated at the top and bottom of Fig. 2.

Figure 2(a) is useful for investigating bifurcations of attractors, but in Fig. 2(b) we also follow unstable solutions and their bifurcations. We can already see that the system features hysteresis at the boundaries of the locking region, which is discussed in more detail below. Figure 2(b) also shows that the extra branches that develop in Fig. 2(a) at $\kappa\tau\geqslant0.1347$ are not bifurcations. They are due to the symmetric limit cycle spiraling through, and thus producing extra crossings with, its value of average intensity.

V. UNSTABLE MANIFOLDS

Figures 3 and 4 show the phase portraits corresponding to Fig. 2, in projection onto (E,N)-space (Fig. 3) and the E-plane (Fig. 4). Except for panels (a) and (b), which were obtained by simulation, these phase portraits were obtained by plotting both branches of the 1D unstable manifold of one of the two symmetric saddle points, marked by $\times$; the corresponding attracting steady states are marked by $+$. The bifurcation diagrams in Fig. 2, along with Figs. 3 and 4, present a complete picture of the route into and out of locking for the PCF laser specified in Sec. II.

For very low values of $\kappa\tau$, system (1) has an almost planar periodic solution surrounding the origin of the E-plane [Figs. 3(a) and 4(a)], which is the continuation of the free-running laser ($\kappa\tau=0$) that has constant power and inversion. With increasing feedback the laser is destabilized. First, the periodic solution starts to curl up near two distinct points [Figs. 3(b) and 4(b)]. It develops a typical shape and does end in a SFH bifurcation when it hits two saddle-focus steady states at $\kappa\tau\approx0.2953$, [Fig. 2(b)]. The exact nature of this global bifurcation is detailed in Sec. VI A. The two saddle-focus steady states are each others symmetric counterparts and are born together with two attractors in the SN bifurcation at $\kappa\tau\approx0.2794$, that is, before the SFH bifurcation [Fig. 2(b)]. This produces a region of bistability between the pair of attracting steady states and the periodic solution. Indeed, for $\kappa\tau\in[0.2794,0.2953]$ one branch of the 1D unstable manifold converges to the periodic solution, while the other branch converges to a locked steady state [Figs. 3(c) and 4(c)]. Physically, this bistability means that the laser is capable of producing locked or periodic output for the same experimental value of $\kappa\tau$, depending on the initial condition. After the SFH bifurcation, bistability is lost and both branches of the saddle-focus steady state converge to one of the two locked solutions, which are the only attractors and

symmetric images of each other [Figs. 3(d) and 4(d)].

This bistability leads to a hysteresis loop: for increasing $\kappa\tau$ the symmetric periodic solution is destroyed in the SFH bifurcation and the system jumps to one of the steady states, whereas for decreasing $\kappa\tau$ the two steady states are destroyed in the SN bifurcation and the system jumps to the symmetric periodic solution. So not only do we see a qualitative change in the attracting solutions, but we also see a change in the symmetry of the attractor, as is indicated in Fig. 2.

As $\kappa\tau$ is increased further through the locking region, the two branches of the 1D unstable manifold of the saddle steady state continue to converge to the respective locked solutions, but with an increasingly larger degree of spiraling [Figs. 3(e)–3(h) and 4(e)–4(h)]. Physically, this spiraling corresponds to the characteristic relaxation oscillations of the laser (a periodic exchange of energy between electric field and inversion), which is still damped. At $\kappa\tau \approx 0.7247$ there is a SL bifurcation creating two pairs of symmetric periodic solutions [Fig. 2(b)], one attracting and one of saddle type. The attracting periodic solutions grow at a rate proportional to the square root of the deviation of $\kappa\tau$ from its value at bifurcation; one speaks of an undamping of the relaxation oscillations. The saddle periodic solutions shrink down to the locked steady state and disappear in a subcritical Hopf bifurcation (H) at $\kappa\tau \approx 0.7487$; see Fig. 2(b). This bifurcation results in the loss of stability of the locked steady states and forms the boundary of the locking range. The system jumps to one of the two attracting periodic solutions and the laser produces self-pulsations (relaxation oscillations). Indeed, both branches of the unstable manifold of the saddle steady state end up at an attracting periodic solution [Figs. 3(j) and 4(j)].

In other words, also the right-hand locking boundary is associated with a region of bistability: for $\kappa\tau \in [0.7247, 0.7487]$ both the pair of locked solutions as well as the pair of periodic solutions corresponding to undamped relaxation oscillations are stable. Again, this leads to a hysteresis loop when $\kappa\tau$ is swept up and down through SL and H.

Note already that the two branches of the unstable manifold of the saddle steady state behave differently just after SL [Figs. 3(i) and 4(i)] and just before H [Figs. 3(j) and 4(j)]. As will be discussed in detail in Sec. VI B, this implies the existence of a heteroclinic bifurcation between SL and H.

When $\kappa\tau$ is increased further, the pair of stable periodic solutions undergoes a period-doubling cascade starting at $\kappa\tau \approx 0.8393$ [Fig. 2(b)]. This eventually leads to both branches of the 1D unstable manifold of the saddle steady state accumulating on a chaotic attractor [Figs. 3(l) and 4(l)]. For even larger values of $\kappa\tau$ the two attractors collide in an attractor crisis caused by a collision of their basins of attraction, culminating in symmetry restoring inside the chaotic region [10].

VI. GLOBAL BIFURCATIONS

We already mentioned in the preceding section that at both boundaries of the locking range we find global bifurcations, namely, a saddle-focus heteroclinic bifurcation between two saddle steady states at the left-hand boundary, and a heteroclinic bifurcation between a saddle steady state and a saddle periodic solution at the right-hand boundary. We now discuss these two global bifurcations in detail.

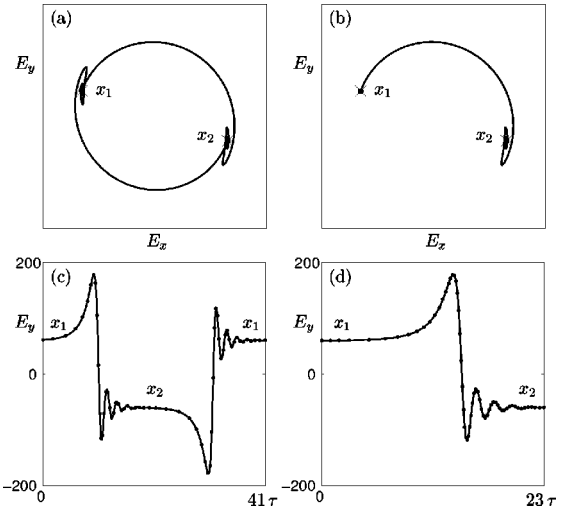

FIG. 5. The periodic solution just before the saddle-focus heteroclinic bifurcation (a) and the heteroclinic connection between the saddle steady states x_1 and x_2 at the bifurcation (b). Panels (c) and (d) show the corresponding time traces of E_y with the mesh points highlighted.

A. Heteroclinic connection between two steady states

In Figure 5(a) we show the symmetric limit cycle just before the SFH bifurcation in which it hits the pair of saddle-focus steady states x_1 and x_2. A time-trace of E_y over its period $\mathsf{T} \approx 41.0\tau$ is shown in Fig. 5(c), where the mesh points used in the DDE-BIFTOOL continuation are highlighted. When approaching the SFH bifurcation the period T goes to infinity. At SFH the periodic solution disappears and instead we have a symmetric pair of heteroclinic connections between x_1 and x_2, one of which is shown in Fig. 5(b). This connecting orbit was computed with the new extension of DDE-BIFTOOL introduced in Ref. [26]. Its time-trace with highlighted mesh points is shown in Fig. 5(d). An analysis of the eigenvalues of the saddle foci shows a negative saddle quantity, $\sigma = \lambda_1 + \mathrm{Re}(\lambda_{2,3})$, where $\lambda_1 > 0$, while $\lambda_{2,3}$ are the complex pair of eigenvalues with negative real part that are closet to the imaginary axis. This implies that there is a unique bifurcating stable limit cycle [22].

The fact that this global bifurcation appears as two simultaneous heteroclinic connections is due to the symmetry of system (1). When one divides out the symmetry and identifies x_1 and x_2 then one gets just a regular saddle-focus homoclinic connection.

We remark that after but near the SFH bifurcation the system is excitable—an example of excitability due to a heteroclinic bifurcation [27]. When the locked solution is perturbed to the other-side of the saddle steady state it will produce a large excursion by following roughly the old heteroclinic connection and ending up at the other locked solution [Figs. 3(d) and 4(d)]. Physically, this corresponds to a

phase jump by π and a relaxing pulse in the power of the laser. We remark that the amplitude of this pulse is quite small. This can also be inferred from Fig. 4(d): the distance from the origin in the *E*-plane does not change much and the power is the square of this distance.

B. Heteroclinic connection between a steady state and a periodic orbit

Between SL and H we have another region of bistability where again the laser can produce qualitatively different stable output depending on the initial condition. The infinite-dimensional stable manifold of the unstable periodic solution forms the boundary between solutions converging to the locked steady state or the stable periodic solution.

As the unstable periodic solution decreases in size there must be a heteroclinic bifurcation located between the two attractors, and we explain this in detail now. Figures 3(i) and 4(i) show the 1D unstable manifolds for $\kappa\tau=0.7252$, which is typical of the region $\kappa\tau\in[0.7247,0.7252]$ where we see one branch spiraling into a periodic solution, while the other branch spirals to a locked solution. However, at $\kappa\tau=0.7253$ [Figs. 3(j) and 4(j)], one branch spirals into a periodic solution as before, but the other branch now spirals out to the symmetric counterpart of this periodic solution. This implies that between the values of $\kappa\tau=0.7252$ and $\kappa\tau=0.7253$ a heteroclinic bifurcation must take place, as is sketched in Fig. 6. Initially, the 1D unstable manifold $W^u(x_0)$ of x_0 spirals into the locked solution [Fig. 6(a)]. As $\kappa\tau$ is increased, the amplitude of the saddle periodic solution Γ_1 starts to decrease, from maximum amplitude at SL to zero amplitude at H, as can be seen in Fig. 2(b). For a particular value of $\kappa\tau, W^u(x_0)$ forms a connection with the stable manifold $W^s(\Gamma_1)$ of the saddle periodic solution Γ_1 [Fig. 6(b)]. As $\kappa\tau$ is increased further this connection is lost and $W^u(x_0)$ spirals out to the attracting periodic solution Γ_2 [Fig. 6(c)]. This behavior is preserved after the subcritical Hopf bifurcation (H): one branch of the saddle steady state converges to a stable periodic solution and the other branch converges to the symmetric counterpart of this periodic solution [Figs. 3(k) and 4(k)].

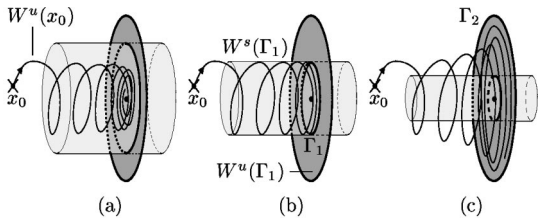

FIG. 6. Before (a), at (b), and after (c) a heteroclinic connection between a saddle steady state x_0 and a saddle periodic solution Γ_1.

VII. DISCUSSION

We studied in detail the transitions into and out of locking of a semiconductor laser with phase-conjugate feedback. Both feature bistabilities that lead to hysteresis loops. Furthermore, both transitions to locking are associated with global bifurcations, namely, a saddle-focus heteroclinic bifurcation and a heteroclinic bifurcation between a steady state and a periodic solution, respectively. Recently developed tools for DDEs allowed us to study these global bifurcations in unprecedented detail.

The bifurcation scenario we described is structurally stable. Initial investigations of some bifurcation curves in the plane of $\kappa\tau$ versus injection current indicate that this scenario appears to be typical for a PCF laser pumped near its threshold current (up to about 7.7% above threshold), which is the region of injection current most commonly investigated in feedback experiments. The construction of a full two-dimensional bifurcation diagram is the next logical step. However, at present this is quite a challenge and requires further developments of numerical methods for DDEs. We are hopeful to report results in this direction in the near future.

Other ongoing investigations of the PCF laser concern the role of periodic solutions and their unstable manifolds in transitions to chaos for larger values of $\kappa\tau$. For a study of the breakup of a torus and a subsequent sudden transition to chaos see Ref. [24].

In more general terms, we believe that the results presented here showcase the usefulness of continuation and manifold computations for the study of DDEs.

ACKNOWLEDGMENTS

The authors thank Koen Engelborghs for his help with DDE-BIFTOOL. B.K. is supported by an ARF grant from the EPSRC of the UK.

[1] G.H.M. van Tartwijk and G.P. Agrawal, Prog. Quantum Electron. **22**, 43 (1998).
[2] B. Krauskopf and D. Lenstra, eds., *Fundamental Issues of Nonlinear Laser Dynamics; Concepts, Mathematics, Physics, and Applications*, AIP Conf. Proc. No. **548** (AIP, Melville, NY, 2000).
[3] A. Gavrielides, in Ref. [2] pp. 191–217.
[4] J. Mørk, B. Tromborg, and J. Mark, IEEE J. Quantum Electron. **28**, 93 (1992).
[5] C.R. Giuliano, Phys. Today **34**(4), 27 (1981).
[6] G.R. Gray, D.H. DeTienne, and G.P. Agrawal, Opt. Lett. **20**, 1295 (1995).
[7] G.P. Agrawal and G.R. Gray, Phys. Rev. A **46**, 5890 (1992).
[8] G.H.M. van Tartwijk, H.J.C. van der Linden, and D. Lenstra, Opt. Lett. **17**, 1590 (1995).
[9] G.R. Gray, D. Huang, and G.P. Agrawal, Phys. Rev. A **49**, 2096 (1994).
[10] B. Krauskopf, G.R. Gray, and D. Lenstra, Phys. Rev. E **58**, 7190 (1998).
[11] X.S. Yao and L. Maleki, Opt. Lett. **22**, 1867 (1997).

[12] T. Heil, I. Fischer, W. Elsäßer, J. Mulet, and C.R. Mirasso, Phys. Rev. Lett. **86**, 795 (2001).
[13] S. A. Gils, S. M. Verduyn Lunel, and H. O. Diekmann, *Delay Equations, Functional-, Complex-, and Nonlinear Analysis* (Springer-Verlag, Berlin, 1995).
[14] J.D. Murray, *Mathematical Biology*, Biomathematics Texts, Vol. 19 (Springer-Verlag, Berlin, 1980).
[15] C.M. Marcus and R.M. Westervelt, Phys. Rev. A **39**, 347 (1989).
[16] H. Glusing-Luerssen, SIAM J. Control Optim. **35**, 480 (1997).
[17] S. M. Verduyn Lunel and B. Krauskopf, in Ref. [2] pp. 66–86.
[18] K. Engelborghs, T. Luzyanina, K. in't Hout, and D. Roose, SIAM J. Sci. Comput. (USA) **22**, 1593 (2000); K. Engelborghs, T. Luzyanina, and D. Roose, J. Comput. Appl. Math. **125**, 265 (2000); K. Engelborghs, DDE-BIFTOOL, http://www.cs.kuleuven.ac.be/~koen/delay/ddebiftool.shtml
[19] C.N. Breton, M. Tetu, and S. Theriault, Opt. Lett. **16**, 1298 (1991).
[20] T. Shimura, M. Tamura, and K. Kuroda, Opt. Lett. **18**, 1645 (1993).
[21] B. Krauskopf, G.H.M. van Tartwijk, and G.R. Gray, Opt. Commun. **177**, 347 (2000).
[22] Y. Kuznetsov, *Elements of Applied Bifurcation Theory* (Springer, Berlin, 1995).
[23] D. Pieroux, T. Erneux, T. Luzyanina, and K. Engelborghs, Phys. Rev. E **63**, 036211 (2001); D. Pieroux, T. Erneux, B. Haegeman, K. Engelborghs, and D. Roose, Phys. Rev. Lett. **87**, 193901 (2001).
[24] K. Green, B. Krauskopf, and K. Engelborghs, Phyisca D (to be published); K. Green and B. Krauskopt, Int. J. Bifurcation Chaos Appl. Sci. Eng. (to be published).
[25] B. Krauskopf, and K. Green, Comp. Phys. (to be published).
[26] G. Samaey, K. Engelborghs, and D. Roose, Dept. of Comp. Sci., K. U. Leuven, Report No. TW 329, 2001, http://www.cs.kuleuven.ac.be/publicaties/rapporten/tw/TW329.abs.html
[27] J.L.A. Dubbeldam, B. Krauskopf, and D. Lenstra, Phys. Rev. E **60**, 6580 (1999).